Electrochemical Activation of Cp* Iridium Complexes for Electrode-driven Water Oxidation Catalysis

Julianne M. Thomsen[1], Stafford W. Sheehan[1], Sara M. Hashmi[2], Jesús Campos[1], Ulrich Hintermair[1,3,], Robert H. Crabtree[1,]*, Gary W. Brudvig[1,]**

1, Department of Chemistry, Yale University, 225 Prospect Street, New Haven, Connecticut 06520, United States

2, Department of Chemical and Environmental Engineering, Yale University, 9 Hillhouse Avenue, New Haven, Connecticut 06520, United States

3, Centre for Sustainable Chemical Technologies, University of Bath, Bath BA2 7AY, United Kingdom

KEYWORDS. Water oxidation, iridium, solar fuels, electrocatalysis.

ABSTRACT. Organometallic iridium complexes bearing oxidatively stable chelate ligands are precursors for efficient homogeneous water oxidation catalysts, but their activity in oxygen evolution has so far been studied almost exclusively with sacrificial chemical oxidants. In this report, we study the electrochemical activation of Cp*Ir complexes and demonstrate true electrode-driven water oxidation catalyzed by a homogeneous iridium species in solution.

Whereas the Cp* precursors exhibit no measurable O_2 evolution activity, the molecular species formed after their oxidative activation are highly active homogeneous water-oxidation catalysts, capable of electrode-driven oxygen evolution with high Faradaic efficiency. We have ruled out the formation of heterogeneous iridium oxides, either as colloids in solution or deposits on the surface of the electrode, and found indication that the conversion of the precursor to the active molecular species occurs by a similar process whether carried out by chemical or electrochemical methods. This work makes these water oxidation catalysts more practical for application in photoelectrochemical dyads for light-driven water splitting.

INTRODUCTION

With global energy demand rising, the need for sustainable and non-polluting energy sources is becoming increasingly urgent.[1] Artificial photosynthesis is a promising strategy for meeting growing energy demands, borrowing a time-tested scheme from nature for the storage of energy from sunlight in the chemical bonds of fuels.[2-4] The crucial half-reaction in both natural and artificial photosynthesis is water oxidation, in which solar energy is used to split two molecules of water into molecular oxygen, electrons, and protons. The protons and electrons harvested from water in this manner can then be used for the formation of sustainable energy carriers and chemical feedstocks.[5] Water oxidation is an endergonic four-electron process with a standard reduction potential of 1.23 V, which in practice, however, requires large additional overpotentials to drive the kinetics. To ease these energetic demands, effective catalysts are needed to make this reaction as efficient as possible. Thus, identifying robust water oxidation catalysts (WOCs) with low overpotentials and high activities has been an active area of research.[6-8]

The number of catalyst candidates for water oxidation has grown substantially in the last ten years.[6,8,9] Among these are the family of Cp*Ir precatalysts introduced by our group in 2009,[10] of which three archetypical members are shown in Chart 1. Solutions initially containing these species were shown to evolve oxygen from water with the addition of an excess of cerium(IV) ammonium nitrate (CAN) or sodium periodate ($NaIO_4$) as sacrificial chemical oxidant. Subsequent reports[11,12] showed the electrochemical behavior of these Cp*Ir complexes in aqueous solution to be consistent with water oxidation catalysis, though there was no definitive assignment by correlation of current with oxygen evolution.

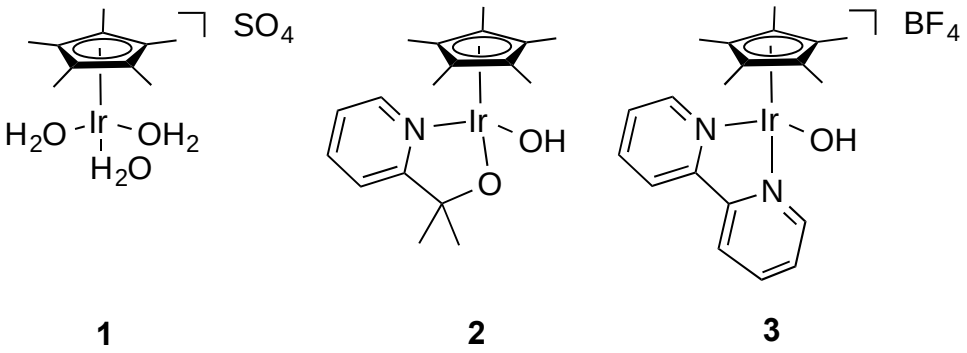

Chart 1. Previously reported iridium precatalysts for catalytic oxygen evolution from water.

Subsequent reports from our groups[13,14] and others[15] noted the rapid formation of characteristic absorption maxima in the range of 570-610 nm in the UV-vis spectra upon the addition of chemical oxidants to Cp*Ir complexes, giving these solutions an intense blue color. Macchioni and co-workers carried out detailed NMR studies of these compounds upon addition of CAN as well as H_2O_2, finding degradation of Cp* to acetic, formic and glycolic acids,[16,17] and others have reported similar findings.[18-20] Our kinetic experiments have shown that the formation of this

blue species correlates with the oxidative removal of the Cp* ligand and onset of oxygen evolution activity,[21] suggesting that the Cp*Ir complexes are catalyst precursors and the blue species are the true active catalysts. Since hydrated iridium(IV) oxides are often blue-colored,[22-27] multiple groups suggested that the blue species generated by chemical oxidation of Cp*Ir complexes could be explained as total degradation of the molecular complexes and polymerization into heterogeneous iridium oxide materials.[15,28] Transmission electron microscopy was most often used to characterize the nanoparticles that were thought to have been formed in the reaction medium. However, the TEM sample preparation procedures and the heating and reducing conditions caused by the high energy electron beam in a TEM may induce particle and cluster formation in initially particle-free samples.[29] We have therefore employed a number of other methods to look for evidence of complex degradation during turnover in solution (*in operando*).[12,14,29,30] We performed time-resolved electrochemical quartz-crystal nanobalance (EQCN) experiments to look for deposition of heterogeneous material during electrochemical oxidation of Cp*Ir complexes,[12] finding that complex **1**, which had been observed to leave blue deposits on electrodes with anodic potential cycling, deposited mass on electrode surfaces when an oxidizing potential was applied. However, complexes **2** and **3**[31] did not yield any such mass deposition, suggesting homogenous catalysis when the 2-(2′-pyridyl)-2-propanoate (pyalc) ligand was present in the precursor. A subsequent study used time-resolved dynamic light scattering (DLS) to monitor particle formation during chemical oxidation in solution, confirming that while complex **1** gave rise to intense scattering characteristic of particle formation within minutes of $NaIO_4$ addition, complexes **2** and **3** did not show any scattering even many hours after oxidation with a large excess of oxidant.[14] This study also showed that changing the concentration of both oxidant and complex significantly affected the size

distribution and rate of formation of particles, as did pH and the presence of soluble salts in the medium, all factors that could complicate the interpretation of findings on similar systems.[15,28]

Recent detailed studies of the homogeneous blue solution formed from $NaIO_4$ and the Cp*Ir complex **2** gave more insights into precursor transformation and confirmed the molecular nature of the blue species.[21] A number of characterization methods, including MALDI-TOF mass spectrometry, X-ray photoelectron spectroscopy (XPS), ^{17}O NMR spectroscopy, and resonance-Raman spectroscopy in conjunction with td-DFT modeling ultimately suggested the active blue species to be a di-μ-oxo iridium(IV,IV) dimer comprising one chelate ligand and two bound waters per iridium center (scheme 1, complex **4**). Importantly, these findings were fully compatible with all previously reported data and observations regardless of their interpretation, including chelate ligand effects on the λ_{max} of the resulting blue solutions and the fact that $(cod)Ir^{I}$ complexes with the same chelate gave results nearly identical to the analogous Cp^*Ir^{III} precursors.[21]

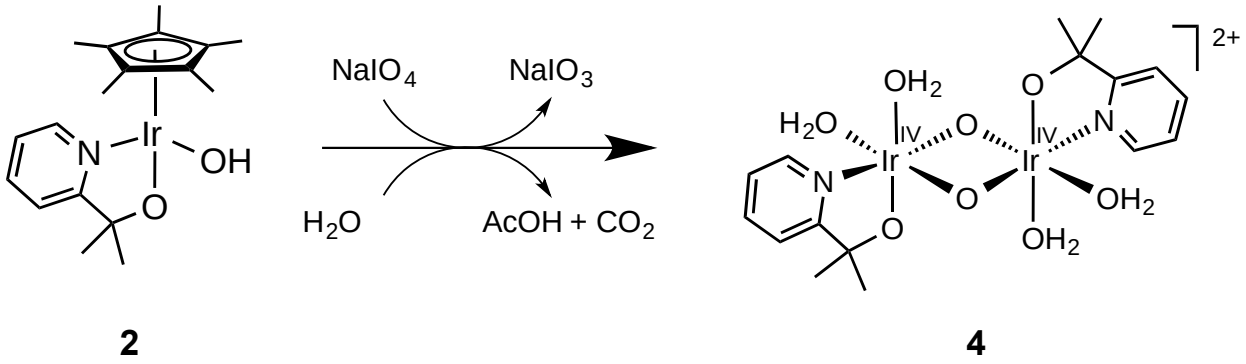

2 **4**

Scheme 1. Reaction of **2** with excess sodium periodate in aqueous solution results in an activated blue species, with the proposed[21] structure shown (**4**).

In photoelectrochemical solar fuel applications, the active catalytic species must be driven in one-electron steps.[32] Use of $NaIO_4$ to drive catalysis is rather inconclusive as to a catalyst's suitability for photoelectrochemical application, as IO_4^- can act as a two-electron

oxidant.[33] Similar one-step, two electron transfer pathways have been hypothesized for other chemical oxidants, such as CAN.[34] Complications such as these, in addition to fundamental differences in their charge transfer reactions, cause chemical oxidants to be rather poor electrode surrogates. These points mean that any promising candidate precatalyst must be examined for electrocatalytic activity once it has been demonstrated to be useful by chemical oxidation. However, this aspect is not often conclusively investigated because these experiments can be more challenging than equivalent trials using chemical oxidants. The timescale of electrochemical water oxidation is typically much slower than when chemical oxidants are used due to the physical limitations imposed by mass transport, electrode surface area and cell geometry.[36] Solution-phase electrocatalysis at electrodes with small surface areas thus necessarily results in low oxygen yields, making accurate, real-time measurement of oxygen evolution difficult. Typically, electrochemical cells must be custom-made in order to couple time-resolved oxygen measurements with electrolysis, and leakage of atmospheric oxygen can cause erroneously high oxygen yields. As a consequence of the logistical challenges of this type of experiment, there are very few reports in the literature of time-correlated measurement of oxygen evolution of solution-phase WOCs driven by electrodes.[37,38]

In this report, we investigate the electrochemical activation of **2** and quantify the electrocatalytic oxygen evolution performance of its activated molecular species by a Clark electrode setup able to detect sub-micromolar changes in O_2 concentration in the liquid phase at high temporal resolution. Significantly, no measurable oxygen is evolved from the precursor complex **2** at the potentials studied. Bulk electrolysis of the precursor species, however, yields a blue solution that is electrocatalytically active for water oxidation, as is the chemically activated version. DLS experiments and electron microscopy show no evidence of heterogeneous particles

or films for either process. Although also a homogeneous system after oxidative activation, clear differences in electrochemical and electrocatalytic behavior are evident when **3** is used as the precursor rather than **2**, whether chemical or electrochemical activation is used, demonstrating that the choice of chelate ligand is important in determining the properties of the active catalyst. Altogether it suggests that both methods of activation yield well-defined molecular species retaining the original chelate ligand, and that the activated molecular species are likely similar regardless of which method is used for activation.

RESULTS AND DISCUSSION

In light of our recent findings on precursor activation with $NaIO_4$,[21] we carefully re-investigated the electrochemical behavior of complexes **2** and **3** to assess their water oxidation activity. If water oxidation was directly accessible as the dominant electrochemical process, it would be expected to show strong pH dependence, with a more basic solution giving rise to an earlier onset of catalytic current or greater current at higher pH,[39] as we have seen before for complex **3**.[11] Cyclic voltammograms (CVs) of aqueous solutions of **2** and **3**, however, showed surprisingly different behaviors in acidic and basic regimes (Figure 1, Figure S1). Under acidic conditions, complex **2** (Figure 1a) had a broad, strongly scan-rate-dependent couple (Figure S1a) centered around 1.0 V vs. NHE, which we assign to Ir(III)/Ir(IV), and a strong irreversible wave at 1.20 V. Under basic conditions, the Ir(III)/Ir(IV) couple shifted to *ca.* 0.70 V with a significant increase in peak separation at all scan rates studied (Figure S1b); the irreversible wave also appeared to have a shoulder at 1.15 V. Surprisingly, however, the potential at which the irreversible wave began to appear did not shift substantially at elevated pH as expected for catalytic water oxidation. Neither did the current at the highest applied voltage (1.50 V) increase

at elevated pH. This was in stark contrast to **3**, which showed significantly different behavior in the two regimes (Figure 1b, Figure S2). The onset of the irreversible wave shifted by approximately 60 mV/pH unit for **3**; however, this irreversible wave did not appear until pH 7.5 (Figure S3). Because bipyridine ligand oxidation has been reported for metal complexes above pH 7[40-42] and this process is known to be pH-dependent, we now ascribe these features of the CV of **3** to bipyridine oxidation rather than water oxidation. The oxidation observed for **3** under basic conditions is interesting in light of the significant body of work performed on Cp*Ir bipyridine complexes.[15,18,28,43,44] The irreversible ligand oxidation process has been described[40,45] as OH^- attack on the bipyridine ring to form a dearomatized radical, followed by oxidative hydroxylation of the ring. Hydroxyl substituents render the bipyridine ring easier to oxidize further, ultimately leading to complete ligand degradation. Consistently, Cp*Ir complexes comprising hydroxo-substituted bipyridine ligands from the start have been seen to degrade to IrO_x when used with CAN.[28] Importantly, however, this electrochemical behavior suggests that the oxidative features observed for both **2** and **3** by CV do not reflect catalytic water oxidation.

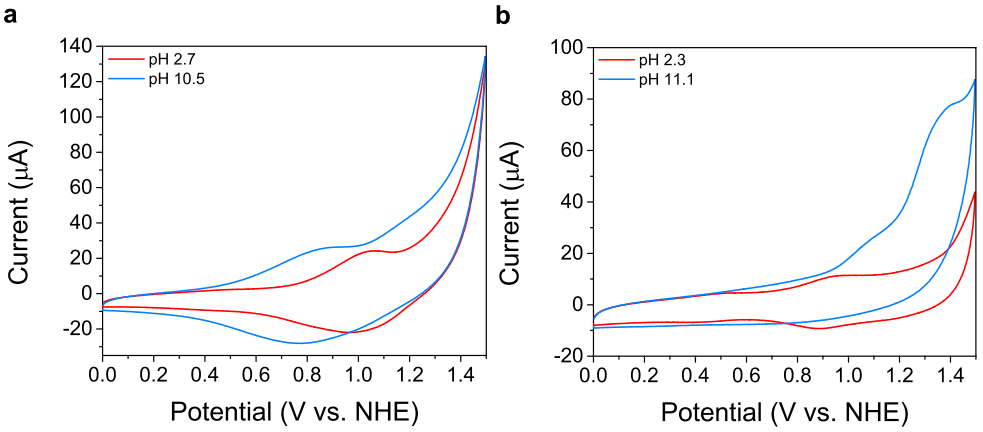

Figure 1. Cyclic voltammograms of (a) 1 mM **2** and (b) 1 mM **3** in acidic and basic pH regimes (conditions: 0.1 M KNO_3 supporting electrolyte pH adjusted with KOH or HNO_3, basal plane graphite working electrode, Ag/AgCl reference electrode, 500 mV/s scan rate).

We then measured the oxygen evolution activity of the precursor **2** compared with its activated blue species **4** generated by prior activation with an excess of $NaIO_4$. Oxygen levels in the liquid phase were quantified by a highly sensitive Clark electrode while stepping the potential up to 1.6 V, which we predicted to be sufficiently high to drive oxygen evolution based on the known reduction potential of $NaIO_4$ (estimated between 1.5-1.6 V vs. NHE at pH 2.5) that does lead to O_2 evolution in the absence of an electrode.[13,46] The electrolyte utilized for these experiments was the $NaIO_3$ that remained in solution after activation of complex **2**,[21] and to control for any electrolyte-related effects the supporting electrolyte used for the precursor **2** was also IO_3^--based. Pre-activation of **2** with 100 equivalents of $NaIO_4$ (0.10 M) caused baseline oxygen levels to be significantly higher than dissolved atmospheric oxygen, so before the oxygen evolution measurements, pre-activated blue species **4** was purged with N_2 to drive off the oxygen evolved during the activation process and then stirred in air to achieve ambient levels of dissolved oxygen. The potential was then held at 0 V vs. NHE for a 10-minute period while baseline oxygen levels were measured, followed by a potential step to 1.6 V, well past the onset of the irreversible wave of **2.** As shown in Figure 2, no oxygen was detected from **2** nor from the control experiment of KIO_3 with no iridium present at this potential, agreeing with the notion that the oxidative features seen in the aqueous CVs of the Cp* complexes do not represent water oxidation. By contrast, pre-activated **4** evolved significant amounts of oxygen with minimal lag phase and a Faradaic efficiency of 59% (±5%) under identical conditions.

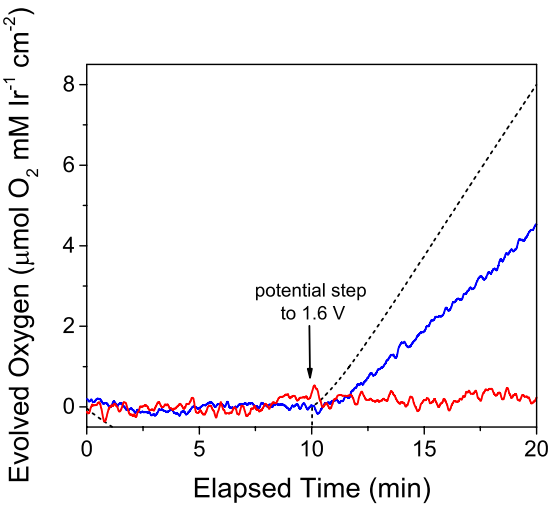

Figure 2. Oxygen evolution over time in response to applied potential at a gold electrode. The electrode was held at 0 V vs. NHE for the first 10 minutes, followed by a step to 1.60 V vs. NHE for the second 10 minutes. Red: 1 mM **2** in 0.1 M KIO_3; blue: 1.2 mM **4** pre-activated with 100 equivalents of $NaIO_4$; dashed black: predicted oxygen from current passed from pre-activated **4**).

It is difficult to calculate a catalyst turnover rate directly from this measurement, because catalysis only occurs within the small reaction layer at the surface of the electrode and therefore only by a very small percentage of the total iridium in solution.[47] Thus, to provide comparable activity metrics evolved oxygen is reported per [Ir] concentration per electrode surface area (0.017 cm^2). The measured rate of oxygen evolution at pH 2.1 for activated **4** was 8.50 (±0.50) nmol O_2 mM Ir^{-1} cm^{-2} s^{-1}, allowing for comparison of relative rates of oxygen evolution from different catalysts and reaction conditions.

Further experiments revealed that oxygen evolution became measurable using our apparatus at an applied potential of 1.45 V vs. NHE, corresponding to an overpotential of 385 mV at pH 2.75. In this context, *overpotential* is defined as the potential at which oxygen evolution is detected via Clark electrode rather than the potential required to achieve a set current

density (in our past work, 0.5 mA/cm^2),[48-50] which is only appropriate for surface-bound catalytic species.[36,51] This is among the lowest overpotentials observed for homogeneous water oxidation catalysts,[37,38,52] although Meyer and co-workers have recently reported base-assisted water oxidation catalysis with an exceedingly low overpotential of 180 mV.[53] Importantly, we have been able to correlate the current passed in our electrochemical experiments in real time with the concomitant formation of O_2 as product. The striking differences between the activated complex **4** and its precursor species **2** highlight the importance of this correlation, with both species showing above-background current but only **4** evolving oxygen.

To ensure that the catalytic activity seen with activated **4** did not arise from iridium oxide deposits formed on the electrode surface during electrolysis (similar to those we have observed from other Cp*Ir precursors such as **1**[12,48]), the electrode was rinsed with deionized water, then placed in a solution of 0.25 M KIO_3 at pH 2.6 and the electrolysis experiment was repeated while monitoring oxygen evolution. This experiment showed negligible levels of current and oxygen evolution, suggesting no active material had deposited on the electrode surface during electrolysis (Figure S7). We also performed post-electrolysis scanning electron microscopy (SEM) and elemental analysis using energy-dispersive X-ray spectroscopy (EDX) of the unpolished electrodes. Again, no deposits of Ir and no coordination of the active catalyst were observed on the surface, with either gold or platinum as the working electrode (Figures S8-9). Use of D_2O rather than H_2O as the solvent during synthesis and then carrying out the electrochemical oxygen evolution experiment revealed a kinetic isotope effect (KIE) of 2.01 by comparing effective rates, which is very distinct from the KIE observed for heterogeneous iridium oxide species (usually no greater than 1-1.1).[54,55]

The Faradaic efficiency of only 59% indicates that water oxidation is not the only process occurring at the electrode surface. In oxygen evolution experiments on **4** formed by $NaIO_4$ pre-activation, residual IO_4^--derived species remain in solution and we were concerned about their possible involvement. It is probable that reduced iodine species such as I_2 are formed by reaction of Cp* partial oxidation products (such as formic acid or methanol) with IO_3^- at acidic pH, and these iodine species are oxidized at lower potentials than water.[56] Such competing processes at the electrode could then result in lower Faradaic efficiency. Another concerning possibility is direct involvement of IO_3^- as a redox mediator for oxygen evolution. As the standard reduction potential of IO_4^- lies close to the potential at which the electrolysis was carried out,[46] it is possible that current passed during electrocatalytic oxygen-evolution could arise from iridium-catalyzed oxidation of IO_3^- to IO_4^-. The regenerated IO_4^- could then react with nearby iridium catalysts to evolve oxygen, so that the overall process would be iodate-mediated water oxidation rather than genuine electrochemical water oxidation by iridium. The active involvement of periodate in oxygen evolution via its dismutation has been discussed[33] but is hard to track experimentally by isotope labeling because of its rapid oxygen exchange in aqueous solution.[13,35,46] Lastly, we were concerned that the chemical oxidants may be directly involved in the formation of the active species,[57] such as by oxygen-atom transfer from IO_4^- to the precursor.[58]

To address these concerns, we attempted bulk electrolysis of **2** to see if it were possible to bypass the use of a chemical oxidant as activator and carry out an electro-oxidation to directly access the activated species **4**. Bulk electrolysis of a stirred aqueous solution of **2** at oxidizing potentials ($E_{app} \geq 1.4$ V vs. NHE) with a high surface area platinum gauze electrode was carried out for extended periods of time. Owing to background currents arising from water oxidation by

the platinum electrode, electrolyses were carried out under acidic conditions (pH 2.3-2.8) to reduce current overloads. Intriguingly, the familiar blue color began to develop shortly after initiation of electrolysis. Experiments varying the applied potential and duration of electrolysis ultimately led to a standard protocol of 36-hour electrolysis of 1-1.25 mM [Ir] at 1.45 V in order to achieve full conversion of the precursor **2** to the blue species (see Supporting Information for complete details). Figure 3a shows UV-vis spectra of **2** before and after electrochemical activation with a broad absorption around 600 nm reminiscent of **4** in the latter (Figure 3b). As in the case of activation by chemical oxidants, the ^{1}H NMR spectrum of this electro-generated blue solution showed the presence of acetic and formic acids from the oxidative degradation of the Cp* ligand (Figure S13). No Cp* resonances were present in the spectrum following bulk electrolysis. Direct comparison of the UV-vis spectra of this electrosynthesized species and chemically synthesized **4** shows some slight differences; certain features are absent in the spectrum of the electrogenerated species, most notably the feature centered around 450 nm. We suspect this absorption is due to aqueous I_2 impurities from activation by $NaIO_4$ in the case of **4**, as I_2 has a substantial absorption in this range.[59]

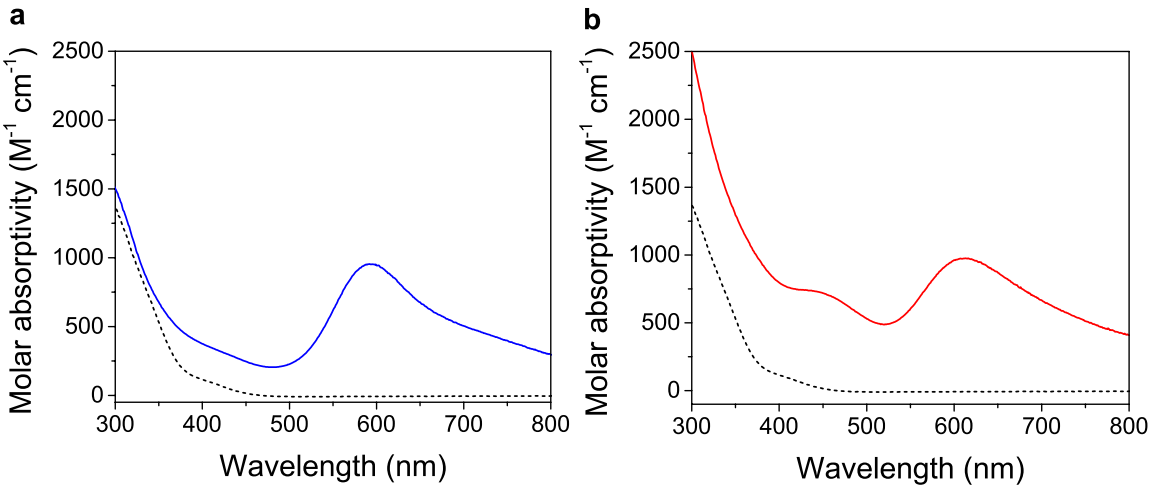

Figure 3. a) UV-vis spectra of **2** before (dashed black) and after (solid blue) 36 hours of electrolysis at a platinum electrode held at 1.45 V vs. NHE in 0.25 M Na_2SO_4 electrolyte at pH 2.6. b) UV-vis spectra of **2** before (dashed black) and 24 hours after (solid red) treatment with 100 equivalents of $NaIO_4$.

Since electrolysis has not only been used for the synthesis of iridium oxide films on electrode surfaces but also for making small IrO_x nanoparticles in solution,[60] we examined the electrosynthesized blue solution by DLS as well as by TEM on dried samples. These data were both gathered for electrolyzed **2** as well as for reference samples of colloidal iridium oxide solutions synthesized following literature procedures.[22,26,27] As iridium concentration is known to have a strong impact on nanoparticle formation,[14] the synthesis was done at 2.5 mM [Ir] and diluted to 1.25 mM [Ir] to compare to the sample prepared by bulk electrolysis (1.25 mM [Ir]). For comparison with previous studies, the standard activation procedure of **2** using 100 equivalents of $NaIO_4$ to yield **4** was also used to make reference DLS samples (again at 2.4 mM and 1.2 mM [Ir]). The sample prepared by electrolysis was essentially indistinguishable from background Na_2SO_4 by DLS, while a discrete correlation function could be fit to the colloid synthesis (Figure S20). Ultrafiltration experiments carried out in tandem with DLS by Fujita and co-workers[61] have suggested that very small particles ($0.5 < x < 2$ nm) that can be trapped by filtration might have escaped detection by DLS, and therefore the DLS measurement may have been inconclusive.[62] Significantly, however, repeated TEM experiments confirmed the lack of particles for electrolyzed **2** at both 2.3 mM and 1.3 mM while revealing very small clusters (~2 nm) in the colloidal solutions synthesized by standard protocols (Figure 4, Figure S10). Thus, electrolytic activation of Cp*Ir precursors with robust chelate ligands may lead to similar molecular species as obtained when chemical oxidants are used. This finding suggests that the

CV features above 1.2 V seen for these complexes reflect incipient precursor activation by Cp* oxidation, which agrees well with the absence of O_2 evolution and the indifference to pH variation (cf. Figure 1). As the fully activated samples exhibit greater current flow at 1.4 V (Figure S11), we further conclude that the initial steps of activating C-H oxidation must be slower than subsequent water oxidation in the fully activated state.

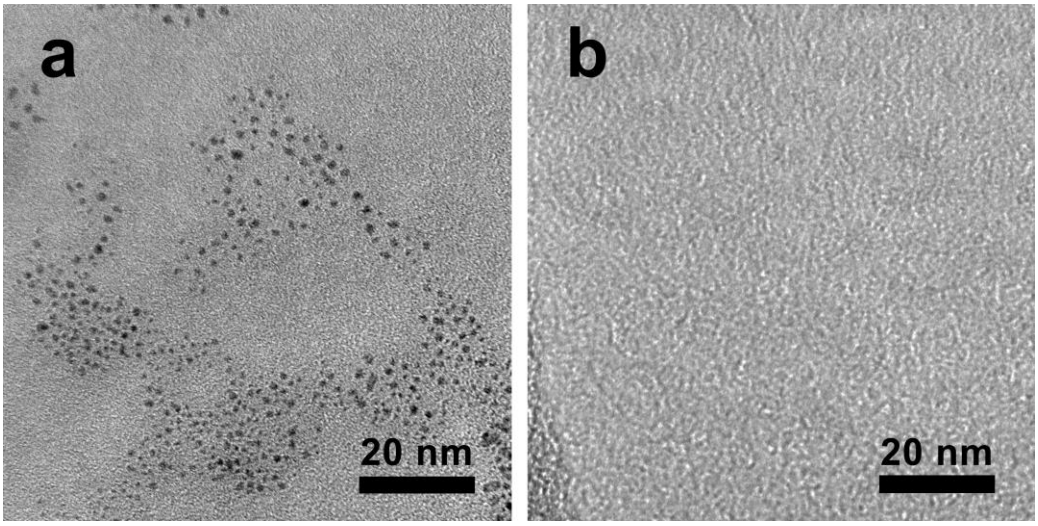

Figure 4. (a) IrO_x nanoparticles of ~2 nm diameter synthesized by aerobic basic hydrolysis of K_2IrCl_6 at 1.25 mM. (b) A sample of **2** at 2.3 mM [Ir] electrolyzed for 36 hours at 1.45 V vs. NHE applied to a TEM grid using the same conditions as in (a), showing no nanoparticles present; no nanoparticles were found anywhere on the grid. Both images were taken using copper TEM grids coated with an ultrathin carbon film (<3 nm) on a lacey carbon support.

To further compare the blue species formed by electrooxidation of **2** to that formed by chemical oxidation, the activity of the electrolyzed solution was examined for electrocatalytic water oxidation. As previously seen with pre-synthesized **4**, oxygen evolution occurred almost immediately, but this time with very high Faradaic efficiency (95% ±5%) at 1.6 V (Figure 5). In the absence of iodine-based electrolytes, the effective rate of oxygen evolution from the

electrosynthesized species also rose to 23 (±0.5) nmol O_2 mM Ir^{-1} cm^{-2} s^{-1}. To the best of our knowledge this is the highest rate reported for electrode-driven oxygen evolution by a solution-phase WOC. At the ambient pH of the solution after electrolysis (pH 1.8-2.3 due to proton production from concomitant water oxidation), oxygen evolution could be seen from applied potentials $\geq$ 1.45 V, or about 345 mV overpotential at pH 2 (Figure S17). In this case the potential required to evolve oxygen was pH-dependent as expected, and raising the pH from 1.9 to 2.9 led to observable oxygen evolution at an applied potential of 1.40 V (figure S17a).

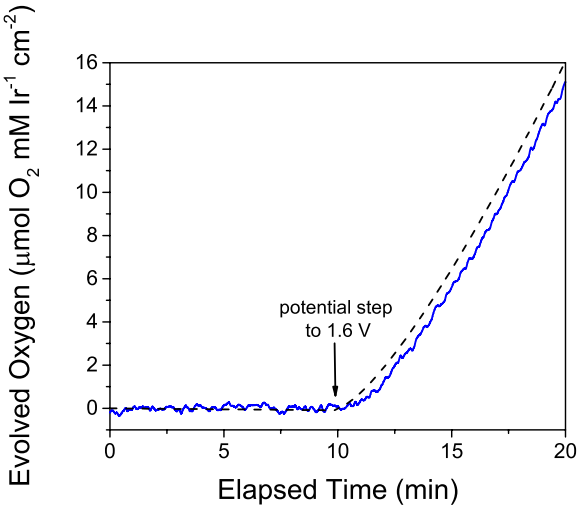

Figure 5. Oxygen evolution from a 2 mM solution of **2** after 36 hours of bulk electrolysis at 1.45 V in 0.25 M Na_2SO_4 (blue: measured by Clark electrode, dashed black: predicted from current passed). A gold electrode was held at 0 V vs. NHE for 10 minutes, then stepped to 1.6 V for 10 minutes.

In addition, the yield of O_2 from the electrosynthesized species was significantly higher than chemically synthesized **4** at the same conditions. Because the effective rate of oxygen evolution of electrosynthesized **4** is nearly three times higher than the effective rate of $NaIO_4$-synthesized **4** at the applied overpotential of 490 mV, the overall oxygen yield increased about threefold (*cf.* Figures 2 and 5). With reference to the CV of $NaIO_4$-synthesized **4** (Figure S4) and

the Pourbaix diagram of IO_4^-,[46,56] we suspected that this could be due to competitive oxidation of residual iodine species rather than water by Ir. Indeed, addition of various amounts of KIO_3 to the electrosynthesized blue species and repeating the measurement supported this hypothesis (Figure 6a). At 0-10 equivalents, the Faradaic yield remained close to 100%. Increasing the quantity of IO_3^- to 50, 100, and 150 equivalents caused a steady reduction in the Faradaic yield, leveling off around 66%, very similar to what was seen with **4** pre-synthesized with $NaIO_4$. The UV-vis spectrum also shifted slightly with increasing amounts of IO_3^-, causing an up to 22 nm red shift of λ_{max} at higher concentrations as well as increased absorbance in the UV range that is characteristic of the $I_2/I^-/I_3^-$ equilibrium in aqueous solution[59,64] (Figure 6b). This is strong evidence that the same active species is formed by both chemical and electrochemical oxidation of **2**, and that differences in properties and catalytic performance between the two solutions arise primarily from iodine-based contaminants present after $NaIO_4$ activation.

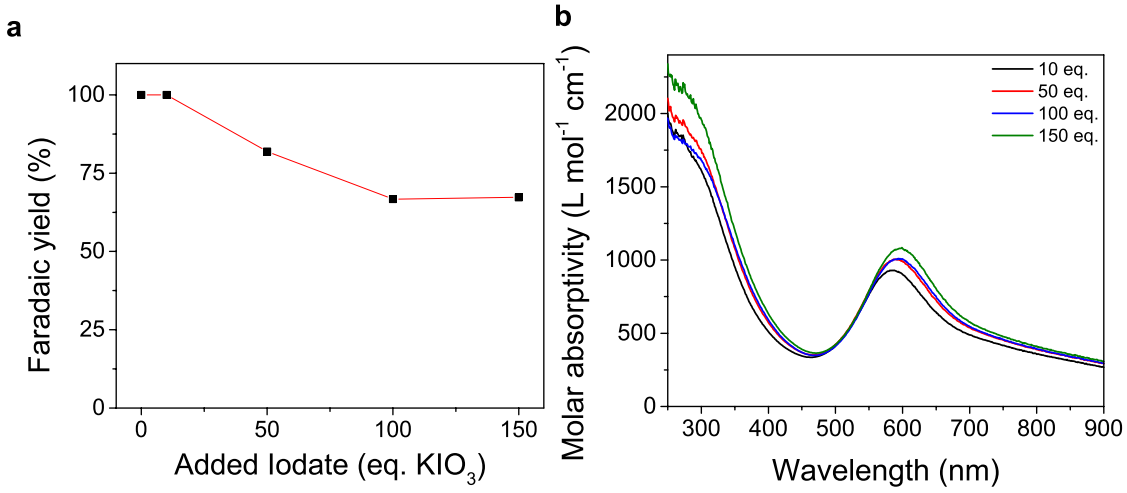

Figure 6. Effect of added KIO_3 on the Faradaic yield of water oxidation (pH 1.9, 1.6 V vs. NHE) with electroactivated **2** (a), and on UV-vis absorbance (b).

Previous studies have shown that the choice of the chelate ligand in the precursor strongly affects the rate of O_2 evolution with $NaIO_4$.[13,21,30] If similar molecular species are formed after electro-activation, this would suggest that ligand effects would also be prominent in electrode-driven oxygen evolution. Therefore an analogous set of experiments to those performed on **2** was carried out for **3**. The species resulting from activation of **3** with 100 equivalents of $NaIO_4$ appeared to be significantly less stable than from **2**, however. Within three hours of $NaIO_4$ addition, the blue color began to fade, and the catalyst solution became a pale green color within six hours. This is likely due to partial reduction under ambient conditions of the blue Ir(IV) species to yellow Ir(III) species, as we have seen before for this compound after $NaIO_4$ treatment.[21] The destabilization of the Ir(IV) state is probably a result of the poorer donor nature of the neutral bipyridine ligand compared to the anionic pyalc ligand. Because activation, purging with N_2, and stirring in air to achieve ambient oxygen levels in the activated solution took some time (see Experimental), it was not possible to carry out electrode-driven oxygen evolution experiments before the solution derived from **3** had lost a significant amount of its blue color. Experiments that were carried out within six hours of $NaIO_4$ addition gave an effective rate of 4.45 (± 0.13) nmol O_2/mM Ir^{-1} cm^{-2} s^{-1} at pH 1.9, about half that observed for the pyalc ligand. In addition, the Faradaic efficiency of activated **3** was only 45% (±5%) at an applied potential of 1.6 V vs. NHE (figure S19), possibly due to an additional step needed for some reduced Ir(III) species to be reoxidized to Ir(IV) in order to enter the catalytic cycle. It is also possible that some of the current at this potential arises from oxidation of the bipyridine ligand, though at the acidic pH used for this study bipyridine oxidation is expected to be very slow.

In addition to the different electrochemical behavior of **3** from **2** after activation with excess $NaIO_4$, precursor **3** also showed very different behavior from **2** in electrochemical

activation. Higher potential (1.55 V) was required to achieve the characteristic blue color, again probably a result of the poorer donor ability of the neutral bipy ligand. As seen with $NaIO_4$, the solution derived from electrolysis of 1 mM **3** lacked the stability of the solution derived from **2**, decaying to a colorless solution within three days of electrolysis. 36 hours of electrolysis of 2 mM **3** at 1.55 V, furthermore, yielded a deep purple solution with a dark precipitate. These clear differences from the species derived from **2** indicate that the choice of chelate ligand has a significant impact on the stability and catalytic properties of the activated species. Together with the previously-mentioned oxidative instability of the bipyridine ligand, **2** seems to be a clearly superior precatalyst for water oxidation than **3**, concomitant with our previous reports that the pyalc ligand assists in providing greater stability and higher activity than bpy for Ir-based water oxidation catalysts. These findings are exciting in that they offer a guideline for molecular tuning of these highly promising water oxidation electro-catalysts.

CONCLUSION

We present evidence for genuine homogeneous electrocatalysis of water oxidation effectively mediated by pre-activated Cp*Ir precatalysts bearing oxidatively stable chelate ligands. The complexes, once activated by Cp* loss using an excess of $NaIO_4$, evolve oxygen with minimal lag phase at electrode surfaces when oxidizing potentials are applied, whereas the precursor complexes before activation with $NaIO_4$ do not evolve any oxygen under the same conditions. Activation of the complexes is also possible using bulk electrolysis at oxidizing potentials $\geq$ 1.4 V vs. NHE, and the product of the activation process appears to be very similar regardless of the oxidative activation method used. The electrochemically-activated species is a highly active catalyst with a very low overpotential of 345 mV and high effective rate of oxygen

evolution. The identity of the chelate ligand has been shown to play a decisive role in the oxygen evolution activity of the activated catalyst as well as the stability of its Ir(IV) state. We emphasize the importance of following real time product detection along with current flow through the working electrode, as in this example we have seen that current observed for precursor species bearing the Cp* ligand does not correspond to oxygen evolution, but likely stems from the oxidation of the sacrificial placeholder ligand Cp*. The reported findings will allow the use the activated species in electrocatalytic applications, with possible extension to integrated photoelectrocatalytic cells as often considered for direct solar fuel generation.

EXPERIMENTAL

General procedures. High purity milli-Q water was used in all experiments. KNO_3, K_2IrCl_6 and Na_2SO_4 ($\geq$99% purity) were purchased from Sigma Aldrich and used as received. $NaIO_4$ and KIO_3 were purchased from Acros Organics and used as received.

Synthesis of [(η^5-Pentamethylcyclopentadienyl)Ir(2-(2'-pyridyl)-2-propanolate-κ^2-O,N)OH]. This compound was prepared similarly to our previously reported procedure.[21] Solid 2-(2'-pyridyl)-2-propanol (82 mg, 0.6 mmol) was added under nitrogen to a freshly prepared solution of [(η^5-Pentamethylcyclopentadienyl)$_2$Ir$_2$(μ-OH)$_3$]OH (0.3 mmol in 20 mL water) and the reaction mixture stirred at room temperature for 16 h. The resulting bright yellow solution was concentrated under reduced pressure to a volume of *ca.* 0.5 mL and then dried under a nitrogen flow. Further drying under high vacuum yielded compound **2** as a fine yellow powder (258 mg, 90%), which was stored under argon.

Synthesis of colloidal iridium oxide solutions. The procedure was carried out according to Murray and co-workers.[26] 2.5 mM K_2IrCl_6 was dissolved in water in a round-bottom flask, then brought to pH 13 with 25% w/v NaOH and immersed in a 90˚ water bath for 20 minutes. During this period color changes of the iridium solution were observed from deep reddish-brown to pale green to pale blue and finally to a pale purple color. After 20 minutes had elapsed, the solution was allowed to cool to room temperature on the bench top and aged for 24 hours before TEM and DLS measurements were taken. We also took an aliquot of this solution, placed it on ice, and added concentrated HCl to achieve a pH of 1 in order to synthesize a species similar to that reported by Mallouk and co-workers.[27]

Electrochemical studies. Electrochemical experiments were all performed using standard three-electrode measurements carried out on a Princeton Applied Research VersaSTAT-4 or a CH Instruments CHI1200B potentiostat. All potentials were measured against Ag/AgCl reference electrodes (+0.197 V vs. NHE) purchased from Bioanalytical Systems, Inc. Working electrodes used were either glassy carbon, gold, or platinum electrodes purchased from Bioanalytical Systems, Inc. or house-made[65] basal plane graphite electrodes. Counter electrodes were platinum wires (for cyclic voltammetry) or platinum mesh (for controlled-potential electrolysis). Before use, electrodes were thoroughly polished with alumina paste and rinsed extensively with Milli-Q water; platinum electrodes were subjected to cycling in 0.5 M sulfuric acid over a potential range of -0.5 to 1.6 V vs. Ag/AgCl before use. Controlled-potential electrolyses for oxygen evolution studies were carried out in a custom water-jacketed glass cell temperature controlled at 25˚ C, with the counter electrode separated from the working and reference electrodes. Gold was used as the working electrode for these studies to minimize background water oxidation relative to platinum and to avoid oxidative damage that glassy

carbon would undergo at the potentials required for oxygen evolution. The surface area of the gold electrode used was 0.017 cm^2. Platinum was also used in control experiments to verify the validity of results obtained with gold and to calibrate the oxygen collection efficiency of the electrochemical cell to ensure accurate calculations of Faradaic efficiency. Iridium complex solutions used for cyclic voltammetry and controlled-potential electrolysis were 1-2 mM in Ir and 0.1-0.2 M in electrolyte, where the electrolyte used was KNO_3 or KIO_3. Bulk electrolysis was carried out using the commercially available bulk electrolysis cell from Bioanalytical Systems, Inc. with a platinum gauze working electrode, Ag/AgCl reference electrode, and platinum mesh counter electrode contained in a separate fritted chamber. The concentration of iridium complex used for electrolysis was 1-2 mM in 0.25 M Na_2SO_4 electrolyte, and pH was adjusted with H_2SO_4 to between 2.4 and 2.9 when electrolysis was initiated. Potential was increased stepwise from 0.5 V to the final voltage (between 1.4 and 1.6 V vs. NHE) in 100-mV steps of 30 seconds each to prevent current overloads. Spectroelectrochemical experiments used the honeycomb cell commercially available from Pine Instruments.

Oxygen evolution measurements. Oxygen evolution data was collected with a YSI 5300A Clark-type electrode using house-written software that averaged 100,000 data points at a rate of 6 per second. The Clark electrode was immersed into a custom water-jacketed glass cell equipped with fittings for the reference, working and counter electrodes. Baseline measurements of water were obtained in this cell before oxygen evolution measurements, and the calibration of voltage reading to concentration of oxygen was made assuming 253 μM dissolved oxygen at 25° C.[66] Baseline slope due to consumption of oxygen by the electrode over time (which becomes evident in longer experiments) was corrected using the control measurements. Iridium catalysts pre-activated with $NaIO_4$ were given sufficient time to allow reaction of all equivalents of IO_4^- in

solution, purged with nitrogen to expel excess dissolved oxygen remaining from synthesis, then stirred in air for a minimum of one hour to re-attain atmospheric dissolved oxygen levels before use in the oxygen assay. Activation and reaction time for **2** was less than for **3**, and solutions of **4** were ready for assay within three hours of $NaIO_4$ addition. Activation time was significantly greater for **3** because of its slower rate of formation and oxygen evolution,[21] and about six hours was required for activation, purging, and oxygen equilibration.

UV-vis spectroscopy. A Varian Cary50 UV-vis spectrophotometer was used for all UV-vis measurements using a 1 cm path length quartz cuvette. Baseline measurements were taken on either neat solvent or blank electrolyte solutions.

Dynamic light scattering measurements. Dynamic light scattering (DLS) experiments were conducted using 532-nm incident laser (Coherent Verdi), at a scattering angle of 90 degrees (ALV5000, ALV-GmbH). Data were collected in intervals of 30 seconds for all samples continuously for 15 minutes in a dark room. The scattered light intensity was monitored throughout, as one indication of the presence of particles. On-board correlator cards (ALV-GmbH) provided the scattered light intensity correlation functions $g(\tau)$ at microsecond resolution. When $g(\tau)$ exhibited a clear exponential decay, signifying diffusive motion and thus the presence of particles, average particle sizes were obtained by cumulant analysis, by fitting to a second-order exponential decay function. Iridium samples were filtered through 0.2 μm filters before DLS analysis to remove any large contaminants. The instrument was calibrated using 320-nm silica bead standards (Bangs Labs) at a range of dilutions to correlate intensity to concentration.

Electron microscopy. SEM and SEM-EDX data were taken using a Hitachi SU-70 analytical scanning electron microscope, and TEM and TEM-EDX data were taken using a FEI

Tecnai Osiris 200 kV transmission electron microscope. Samples were prepared by applying aqueous solutions of iridium compounds onto a TEM grid and ambient drying. Each sample was investigated three times using different types of TEM grids (silicon monoxide, 5-10 nm carbon, and ultrathin carbon on a lacey carbon support; all from Ted Pella) and different preparatory procedures, including sonication or centrifugation, to thoroughly determine whether or not solutions contained nanoparticles.

ASSOCIATED CONTENT

Supporting Information. Additional electrochemical data, UV-visible spectra, electron microscopy, dynamic light scattering and oxygen evolution data. This material is available free of charge via the Internet at http://pubs.acs.org.

AUTHOR INFORMATION

Corresponding Author

robert.crabtree@yale.edu; gary.brudvig@yale.edu; u.hintermair@bath.ac.uk

Author Contributions

The manuscript was written through contributions of all authors. All authors have given approval to the final version of the manuscript.

Funding Sources

This work was partially supported as part of the Argonne-Northwestern Solar Energy Research (ANSER) Center, an Energy Frontier Research Center funded by the U.S. Department of Energy, Number DE-SC0001059 (J.M.T., R.H.C. and G.W.B.), as well as the National Science

Foundation via a Graduate Research Fellowship and NSF MRSEC DMR 1119826 (S.W.S.). J.C. acknowledges a catalysis grant from the Division of Chemical Sciences, Geosciences, and Biosciences, Office of Basic Energy Sciences of the U.S. Department of Energy through grant DE-FG02-84ER13297. U.H. acknowledges support from the Alexander von Humboldt Foundation through a Feodor Lynen Research Fellowship and from the Centre for Sustainable Chemical Technologies at the University of Bath for a Whorrod Research Fellowship.

ACKNOWLEDGMENT

We thank Drs. James D. Blakemore, Alec C. Durrell and Karin J. Young for helpful discussions. J.M.T. thanks Daryl Smith for fabrication of custom glassware and Rosario Bernardo for machined parts.

REFERENCES

(1) Lewis, N. S.; Nocera, D. G. *Proc. Natl. Acad. Sci. U. S. A.* **2006**, *103*, 15729.

(2) Blankenship, R. E.; Tiede, D. M.; Barber, J.; Brudvig, G. W.; Fleming, G.; Ghirardi, M.; Gunner, M. R.; Junge, W.; Kramer, D. M.; Melis, A.; Moore, T. A.; Moser, C. C.; Nocera, D. G.; Nozik, A. J.; Ort, D. R.; Parson, W. W.; Prince, R. C.; Sayre, R. T. *Science* **2011**, *332*, 805.

(3) Meyer, T. J. *Acc. Chem. Res.* **1989**, *22*, 163.

(4) Alstrum-Acevedo, J. H.; Brennaman, M. K.; Meyer, T. J. *Inorg. Chem.* **2005**, *44*, 6802.

(5) Gust, D.; Moore, T. A.; Moore, A. L. *Acc. Chem. Res.* **2009**, *42*, 1890.

(6) Yagi, M.; Kaneko, M. *Chem. Rev.* **2001**, *101*, 21.

(7) Wasylenko, D. J.; Palmer, R. D.; Berlinguette, C. P. *Chem. Comm.* **2013**, *49*, 218.

(8) Yagi, M.; Syouji, A.; Yamada, S.; Komi, M.; Yamazaki, H.; Tajima, S. *Photochem. Photobiol. Sci.* **2009**, *8*, 139.

(9) *Molecular Water Oxidation Catalysis: A Key Topic for New Sustainable Energy Conversion Schemes*; Llobet, A., Ed.; John Wiley & Sons, Ltd: Chichester, UK, 2014.

(10) Hull, J. F.; Balcells, D.; Blakemore, J. D.; Incarvito, C. D.; Eisenstein, O.; Brudvig, G. W.; Crabtree, R. H. *J. Am. Chem. Soc.* **2009**, *131*, 8730.

(11) Blakemore, J. D.; Schley, N. D.; Balcells, D.; Hull, J. F.; Olack, G. W.; Incarvito, C. D.; Eisenstein, O.; Brudvig, G. W.; Crabtree, R. H. *J. Am. Chem. Soc.* **2010**, *132*, 16017.

(12) Schley, N. D.; Blakemore, J. D.; Subbaiyan, N. K.; Incarvito, C. D.; D'Souza, F.; Crabtree, R. H.; Brudvig, G. W. *J. Am. Chem. Soc.* **2011**, *133*, 10473.

(13) Parent, A. R.; Brewster, T. P.; De Wolf, W.; Crabtree, R. H.; Brudvig, G. W. *Inorg. Chem.* **2012**, *51*, 6147.

(14) Hintermair, U.; Hashmi, S. M.; Elimelech, M.; Crabtree, R. H. *J. Am. Chem. Soc.* **2012**, *134*, 9785.

(15) Grotjahn, D. B.; Brown, D. B.; Martin, J. K.; Marelius, D. C.; Abadjian, M.-C.; Tran, H. N.; Kalyuzhny, G.; Vecchio, K. S.; Specht, Z. G.; Cortes-Llamas, S. A.; Miranda-Soto, V.; van Niekerk, C.; Moore, C. E.; Rheingold, A. L. *J. Am. Chem. Soc.* **2011**, *133*, 19024.

(16) Savini, A.; Belanzoni, P.; Bellachioma, G.; Zuccaccia, C.; Zuccaccia, D.; Macchioni, A. *Green Chem.* **2011**, *13*, 3360.

(17) Zuccaccia, C.; Bellachioma, G.; Bolaño, S.; Rocchigiani, L.; Savini, A.; Macchioni, A. *Eur. J. Inorg. Chem.* **2012**, *2012*, 1462.

(18) Wang, C.; Wang, J.-L.; Lin, W. *J. Am. Chem. Soc.* **2012**, *134*, 19895.

(19) Park-Gehrke, L. S.; Freudenthal, J.; Kaminsky, W.; DiPasquale, A. G.; Mayer, J. M. *Dalton Trans.* **2009**, 1972.

(20) Ingram, A. J.; Wolk, A. B.; Flender, C.; Zhang, J.; Johnson, C. J.; Hintermair, U.; Crabtree, R. H.; Johnson, M. A.; Zare, R. N. *Inorg. Chem.* **2014**, *53*, 423.

(21) Hintermair, U.; Sheehan, S. W.; Parent, A. R.; Ess, D. H.; Richens, D. T.; Vaccaro, P. H.; Brudvig, G. W.; Crabtree, R. H. *J. Am. Chem. Soc.* **2013**, *135*, 10837.

(22) Harriman, A.; Thomas, J. M.; Millward, G. R. *New J. Chem.* **1987**, *11*, 757.

(23) Castillo-Blum, S. E.; Richens, D. T.; Sykes, A. G. *Chem. Comm.* **1986**, 1120.

(24) Castillo-Blum, S. E.; Richens, D. T.; Sykes, A. G. *Inorg. Chem.* **1989**, *28*, 954.

(25) Nakagawa, T.; Beasley, C. A.; Murray, R. W. *J. Phys. Chem. C* **2009**, *113*, 12958.

(26) Gambardella, A. A.; Bjorge, N. S.; Alspaugh, V. K.; Murray, R. W. *J. Phys. Chem. C* **2011**, *115*, 21659.

(27) Zhao, Y. X.; Hernandez-Pagan, E. A.; Vargas-Barbosa, N. M.; Dysart, J. L.; Mallouk, T. E. *J. Phys. Chem. Lett.* **2011**, *2*, 402.

(28) Hong, D.; Murakami, M.; Yamada, Y.; Fukuzumi, S. *Energy Environ. Sci.* **2012**, *5*, 5708.

(29) Crabtree, R. H. *Chem. Rev.* **2012**, *112*, 1536.

(30) Codolà, Z.; M S Cardoso, J.; Royo, B.; Costas, M.; Lloret-Fillol, J. *Chem. Eur. J.* **2013**, *19*, 7203.

(31) Blakemore, J. D., California Institute of Technology, Pasadena, CA. Personal communication, 2014.

(32) Young, K. J.; Martini, L. A.; Milot, R. L.; Snoeberger, R. C.; Batista, V. S.; Schmuttenmaer, C. A.; Crabtree, R. H.; Brudvig, G. W. *Coord. Chem. Rev.* **2012**, *256*, 2503.

(33) Hetterscheid, D. G. H.; Reek, J. N. H. *Eur. J. Inorg. Chem.* **2014**, *2014*, 742.

(34) Ikeda-Ohno, A.; Tsushima, S.; Hennig, C.; Yaita, T.; Bernhard, G. *Dalton Trans.* **2012**, *41*, 7190.

(35) Pecht, I.; Luz, Z. *J. Am. Chem. Soc.* **1965**, *87*, 4068.

(36) Bard, A. J.; Faulkner, L. R. *Electrochemical methods: fundamentals and applications*; 2nd ed.; Wiley: New York, 2001.

(37) Barnett, S. M.; Goldberg, K. I.; Mayer, J. M. *Nature chemistry* **2012**, *4*, 498.

(38) Wang, D.; Groves, J. T. *Proc. Natl. Acad. Sci. U. S. A.* **2013**, *110*, 15579.

(39) Pourbaix, M. *Atlas of electrochemical equilibria in aqueous solutions*; National Association of Corrosion Engineers, 1974.
(40) Ghosh, P. K.; Brunschwig, B. S.; Chou, M.; Creutz, C.; Sutin, N. *J. Am. Chem. Soc.* **1984**, *106*, 4772.
(41) Liu, F.; Concepcion, J. J.; Jurss, J. W.; Cardolaccia, T.; Templeton, J. L.; Meyer, T. J. *Inorg. Chem.* **2008**, *47*, 1727.
(42) Hurst, J. K. *Coord. Chem. Rev.* **2005**, *249*, 313.
(43) Depasquale, J.; Nieto, I.; Reuther, L. E.; Herbst-Gervasoni, C. J.; Paul, J. J.; Mochalin, V.; Zeller, M.; Thomas, C. M.; Addison, A. W.; Papish, E. T. *Inorg. Chem.* **2013**, *52*, 9175.
(44) Zhang, T.; deKrafft, K. E.; Wang, J.-L.; Wang, C.; Lin, W. *Eur. J. Inorg. Chem.* **2014**, *2014*, 698.
(45) Limburg, B.; Bouwman, E.; Bonnet, S. *Coord. Chem. Rev.* **2012**, *256*, 1451.
(46) Parent, A. R.; Crabtree, R. H.; Brudvig, G. W. *Chem. Soc. Rev.* **2013**, *42*, 2247.
(47) Costentin, C.; Drouet, S.; Robert, M.; Savéant, J.-M. *J. Am. Chem. Soc.* **2012**, *134*, 11235.
(48) Blakemore, J. D.; Schley, N. D.; Olack, G. W.; Incarvito, C. D.; Brudvig, G. W.; Crabtree, R. H. *Chem. Sci.* **2011**, *2*, 94.
(49) Kushner-Lenhoff, M. N.; Blakemore, J. D.; Schley, N. D.; Crabtree, R. H.; Brudvig, G. W. *Dalton Trans.* **2013**, *42*, 3617.
(50) Sheehan, S. W.; Thomsen, J. M.; Hintermair, U.; Crabtree, R. H.; Brudvig, G. W.; Schmuttenmaer, C. A. *Nat. Chem.* **2014**, submitted.
(51) Fourmond, V.; Jacques, P.-A.; Fontecave, M.; Artero, V. *Inorg. Chem.* **2010**, *49*, 10338.
(52) Zhang, T.; Wang, C.; Liu, S.; Wang, J.-L.; Lin, W. *J. Am. Chem. Soc.* **2013**, *136*, 273.
(53) Tamaki, Y.; Vannucci, A. K.; Dares, C. J.; Binstead, R. A.; Meyer, T. J. *J. Am. Chem. Soc.* **2014**, *136*, 6854.
(54) Hara, M.; Waraksa, C. C.; Lean, J. T.; Lewis, B. A.; Mallouk, T. E. *J. Phys. Chem. A* **2000**, *104*, 5275.
(55) Hoertz, P. G.; Kim, Y.-I.; Youngblood, W. J.; Mallouk, T. E. *J. Phys. Chem. B* **2007**, *111*, 6845.
(56) Ticknor, K. V.; Cho, Y. H. *Journal of Radioanalytical and Nuclear Chemistry, Articles* **1990**, *140*, 75.
(57) Connelly, N. G.; Geiger, W. E. *Chem. Rev.* **1996**, *96*, 877.
(58) Turlington, C. R.; White, P. S.; Brookhart, M.; Templeton, J. L. *J. Am. Chem. Soc.* **2014**, *136*, 3981.
(59) Naorem, H.; Devi, S. D. *Spectrochim. Acta Part A Mol. Biomol. Spectrosc.* **2013**, *101*, 67.
(60) Nakagawa, T.; Bjorge, N. S.; Murray, R. W. *J. Am. Chem. Soc.* **2009**, *131*, 15578.
(61) Lewandowska-Andralojc, A.; Polyansky, D. E.; Wang, C. H.; Wang, W. H.; Himeda, Y.; Fujita, E. *Phys Chem Chem Phys* **2014**, *Advance Article*.
(62) .
(63) Rose, D.; Lever, F. M.; Powell, A. R.; Wilkinson, G. *J. Chem. Soc. A* **1969**, 1690.
(64) Li, N.; Shi, L.; Wang, X.; Guo, F.; Yan, C. *International Journal of Analytical Chemistry* **2011**, *2011*.

(65) Cady, C. W.; Shinopoulos, K. E.; Crabtree, R. H.; Brudvig, G. W. *Dalton Trans.* **2010**, *39*, 3985.
(66) Truesdale, G. A.; Downing, A. L. *Nature* **1954**, *173*, 1236.